

Article

Flexural and Shear Performance of Prestressed Composite Slabs with Inverted Multi-Ribs

Sun-Jin Han ¹, Jae-Hoon Jeong ¹, Hyo-Eun Joo ¹, Seung-Ho Choi ¹, Seokdong Choi ² and Kang Su Kim ^{1,*}

¹ Department of Architectural Engineering, University of Seoul, 163 Seoulsiripdaero, Dongdaemun-gu, Seoul 02504, Korea; sjhan1219@gmail.com (S.-J.H.); ghostwise@naver.com (J.-H.J.); hyoyjoo@gmail.com (H.-E.J.); ssarmilmil@gmail.com (S.-H.C.)

² Yunwoo Structural Engineers Co., Ltd., 4F, Tower B, 128, Beobwon-ro, Songpa-gu, Seoul 05854, Korea; csd@yunwoo.co.kr

* Correspondence: kangkim@uos.ac.kr; Tel.: +82-2-6490-2762; Fax: +82-2-6490-2749

Received: 28 October 2019; Accepted: 13 November 2019; Published: 17 November 2019



Abstract: Half precast concrete slabs with inverted multi-ribs (Joint Advanced Slab, JAS), which enhance composite performance between slabs by introducing shear keys at connections between the slabs and improve structural performance by placing prestressing tendons and truss-type shear reinforcements, have recently been developed and applied in many construction fields. In this study, flexural and shear tests were performed to verify the structural performance of JAS members. Towards this end, two flexural specimens and four shear specimens were fabricated, and the presence of cast-in-place concrete and the location of the critical section were set as the main test variables. In addition, the flexural and shear performance of the JAS was quantitatively evaluated using a non-linear flexural analysis model and current structural design codes. Evaluation results confirmed that the flexural behavior of the JAS was almost similar to the behavior simulated through the non-linear flexural analysis model, and the shear performance of the JAS can also be estimated appropriately by using the shear strength equations presented in the current design codes. For the JAS with cast-in-place concrete, however, the shear strength estimation results differed significantly depending on the way that the shear contributions of the precast concrete unit and cast-in-place concrete were calculated. Based on the analysis results, this study proposed a design method that can reasonably estimate the shear strength of the composite JAS.

Keywords: inverted multi tee; prestressed concrete; precast concrete; structural performance; flexural analysis; shear strength

1. Introduction

The precast concrete (PC) slab has many advantages in terms of the quality control of concrete through prefabrication at the factory, reduction of construction costs by shortening the construction period, and reduction of waste on construction sites [1–3]. Accordingly, various types of half-PC slab members, such as the flat precast slab, hollow-core slab, multi-rib slab, and double-tee slab, have been developed, and related research on them has been actively done. The flat precast slab has the advantage of ensuring easy mold operation and rebar placement. However, because of the thin flanges, it requires temporary work, such as the installation of shores, to resist the construction load at the time of casting topping concrete [4,5]. The hollow-core slab can reduce the lifting weight because of the presence of hollows in the cross-section and can greatly increase the thickness of the cross-section under design conditions in which a load is quite large [3,6–8]. However, the hollow-core slab manufactured using an extruder is very vulnerable to web shear at the end of the member because shear reinforcement

cannot be placed on the web [3,9,10]. Furthermore, since the ACI 318-14 code [11] prescribes that the web shear strength of a one-way prestressed member that exceeds 315 mm in thickness and has less than the minimum shear reinforcement shall be reduced by half, the application of the hollow-core slab produced by the extrusion method can provide non-economical design results [3,10]. Meanwhile, the multi-rib and double-tee slabs have cross-sectional shapes that are very efficient for positive moment resistance because of the removal of an unnecessary concrete section on the tension side. However, there is a disadvantage in that the top flange is very thin, making it difficult to achieve continuity at the member ends [12–14].

In order to maximize the advantages of the half-PC system, a joint advanced slab (JAS) to minimize the temporary work process and lifting weight during construction, and facilitate the placement of shear reinforcement, has recently been developed, as shown in Figure 1. The JAS has advantages, in that it has greater flexural stiffness of the cross-section than that of the flat precast slab because of the presence of inverted multi-ribs, and it can minimize the on-site rebar placement process, because the shear keys introduced at both ends of the slab panel replace the reinforcing steel required for connections between PC slabs. In addition, the introduction of prestressing into the cross-section improves the flexural and shear performance of the member, and the N-type lattice reinforcement is placed in the ribs as a stirrup to resist horizontal and vertical shear forces effectively. Moreover, since the JAS ensures continuity at the end region of the slab, it can resist the entire static moment generated by the load applied after the placement of cast-in-situ concrete by dividing it into positive and negative moments.

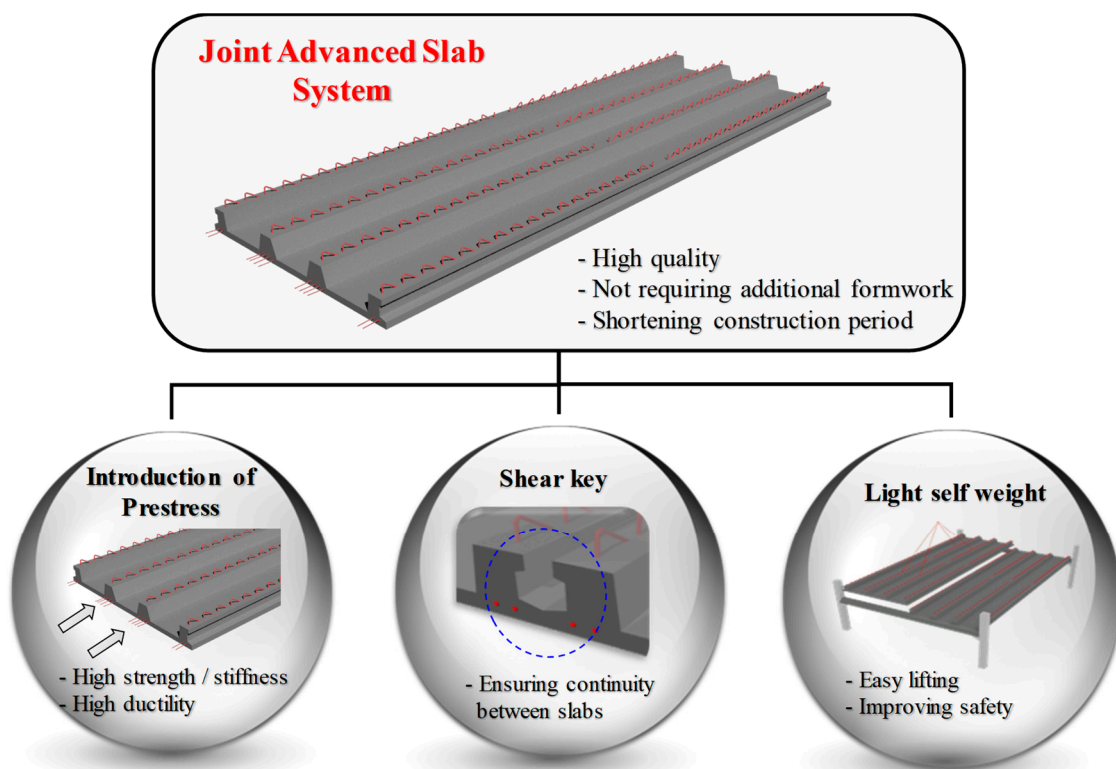


Figure 1. Characteristics of the joint advanced slab (JAS).

In this regard, experimental research was done to examine the flexural and shear performance of the newly developed JAS, where the presence of cast-in-place concrete and the location of the critical section were set as the main test variables. For the flexural specimens, the strain gauges were attached to the longitudinal tension reinforcement and concrete in a compression zone and were attached to the stirrups for the shear specimens. Then, the member behavior, according to the loads, was measured and analyzed in detail. In addition, this study quantitatively evaluated the flexural and shear performance

of the JAS by comparing the test results and analysis results from the non-linear flexural analysis model and structural design codes. In particular, based on the shear test results, a method to reasonably estimate the shear contributions of the PC unit and cast-in-place concrete was proposed for the shear design of the JAS.

2. Experimental Program

2.1. Test Specimens

Table 1 and Figure 2 show the details of the test specimens. A total of six specimens, one PC unit flexural specimen, one PC flexural specimen with cast-in-place concrete two PC unit shear specimens, and two PC shear specimens with cast-in-place concrete, were fabricated to evaluate the structural performance of the JAS. The width (b) and length (L) of all specimens were 1100 mm and 7200 mm, respectively, and six prestressing strands with a diameter of 15.2 mm were placed on the tension side of the specimens. In addition, the N-type lattice reinforcement with a diameter of 10 mm and a spacing of 200 mm was placed in inverted multi ribs. The PC unit flexural and shear specimens were named UF(Unit-Flexural) and US(Unit-Shear), and the flexural and shear specimens with cast-in-place concrete were named CF(Composite-Flexural) and CS(Composite-Shear), respectively. Since the JAS is manufactured through the pretension method, a transfer length zone exists, and the stress of the strands in this region is smaller than the effective prestress (f_{se}). Therefore, for the US and CS specimens, shear tests were conducted in the transfer length zone and the strain plateau zone, respectively, as shown in Figure 3. To distinguish between the test specimens, 't' and 'f' were added to each of the specimen names. Here, the USf and CSf specimens were additionally strengthened with eight 19 mm diameter rebars on the tension side, in order to avoid flexural failure and to induce shear failure. The magnitude of the effective prestress (f_{se}) introduced in the specimen was 61% of the ultimate strength (f_{pu}) of the tendon. The concrete compressive strength (f_c') of the PC unit specimens was 27.0 MPa, and the PC compressive strength in the composite specimens was 36.0 MPa. In addition, the compressive strengths of the cast-in-place concrete were 18.5 and 21.3 MPa, respectively. It is noted that the designed compressive strengths of PC and cast-in-place concrete were 40 and 30 MPa, respectively; however, the compressive strengths were found to be smaller than the designed compressive strengths because the outdoor air temperature was below zero degree Celsius during the fabrication of the specimens [15].

Table 1. Details of the test specimens.

Specimen	Description	Test Region	h (mm) ***	d_p, d_s (mm) ***	A_{ps}, A_s (mm ²) ***		Stirrups **	f_c' (MPa) ***	
					Strands *	Rebar **		PC	Topping
UF	Flexure (without topping)	-	230	190	6- Φ 15.2 (832.2)	-		27.0	-
CF	Flexure (with topping)	-	330	290	6- Φ 15.2 (832.2)	-	D10@200 + D10@200 (inclined)	36.0	21.3
USt	Shear (without topping)	Transfer length zone	230	190	6- Φ 15.2 (832.2)	-		27.0	-
USf	Shear (without topping)	Strain plateau zone	230	190	6- Φ 15.2 (832.2)	8-D19 (2288)		27.0	-
CSSt	Shear (with topping)	Transfer length zone	330	290	6- Φ 15.2 (832.2)	8-D19 (2288)		36.0	18.5
CSf	Shear (with topping)	Strain plateau zone	330	290	6- Φ 15.2 (832.2)	8-D19 (2288)		36.0	18.5

* Tensile strength of the prestressing strands (f_{pu}) was 1936 MPa. ** Yield strengths of the tensile reinforcement (f_y) and stirrup (f_{vy}) were 503 and 406 MPa, respectively. *** Notations: h : member height, d_s : effective depth, A_{ps} : sectional area of strands, A_s : sectional area of tensile reinforcement, f_c' : compressive strength of concrete.

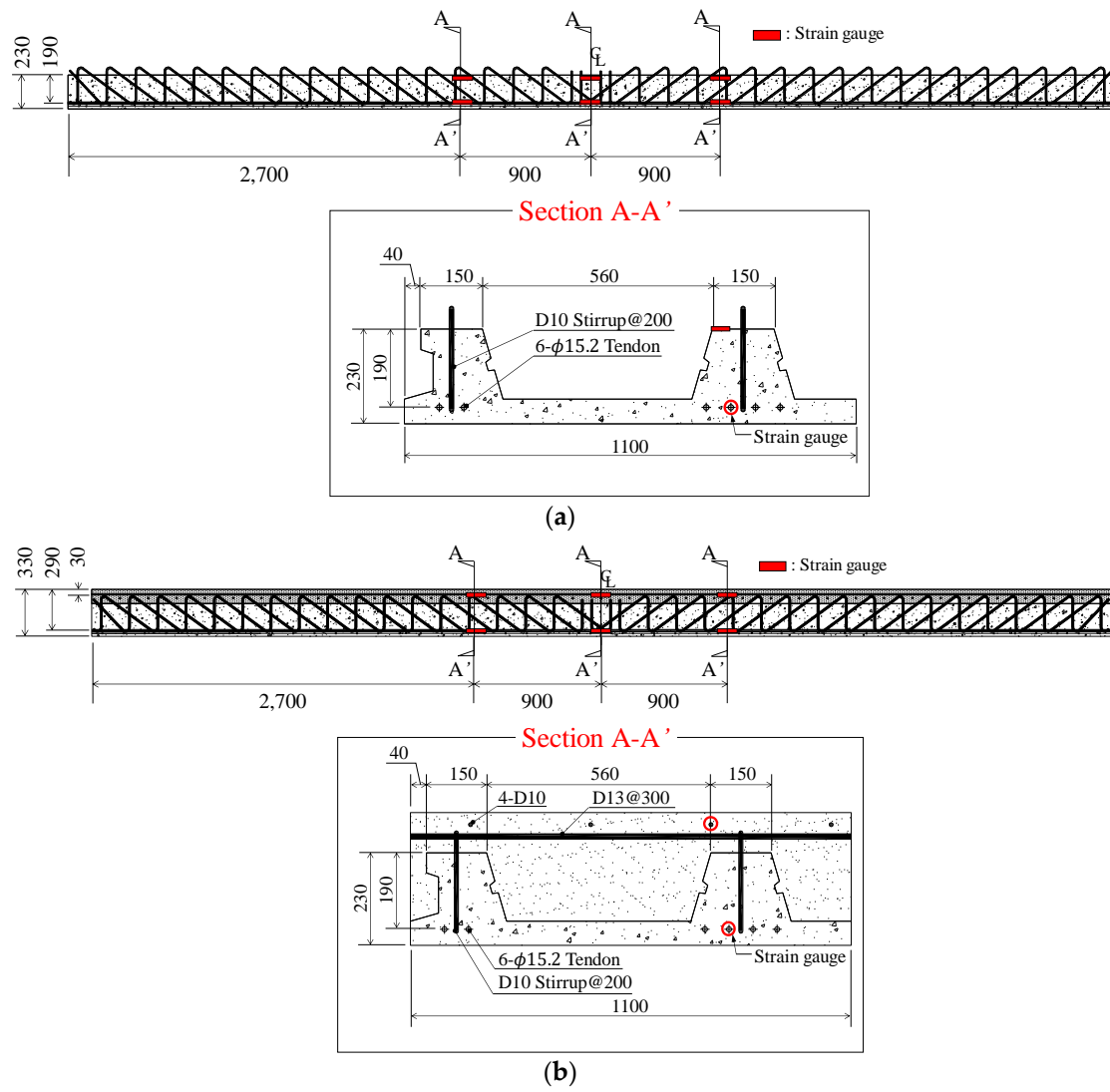


Figure 2. Cont.

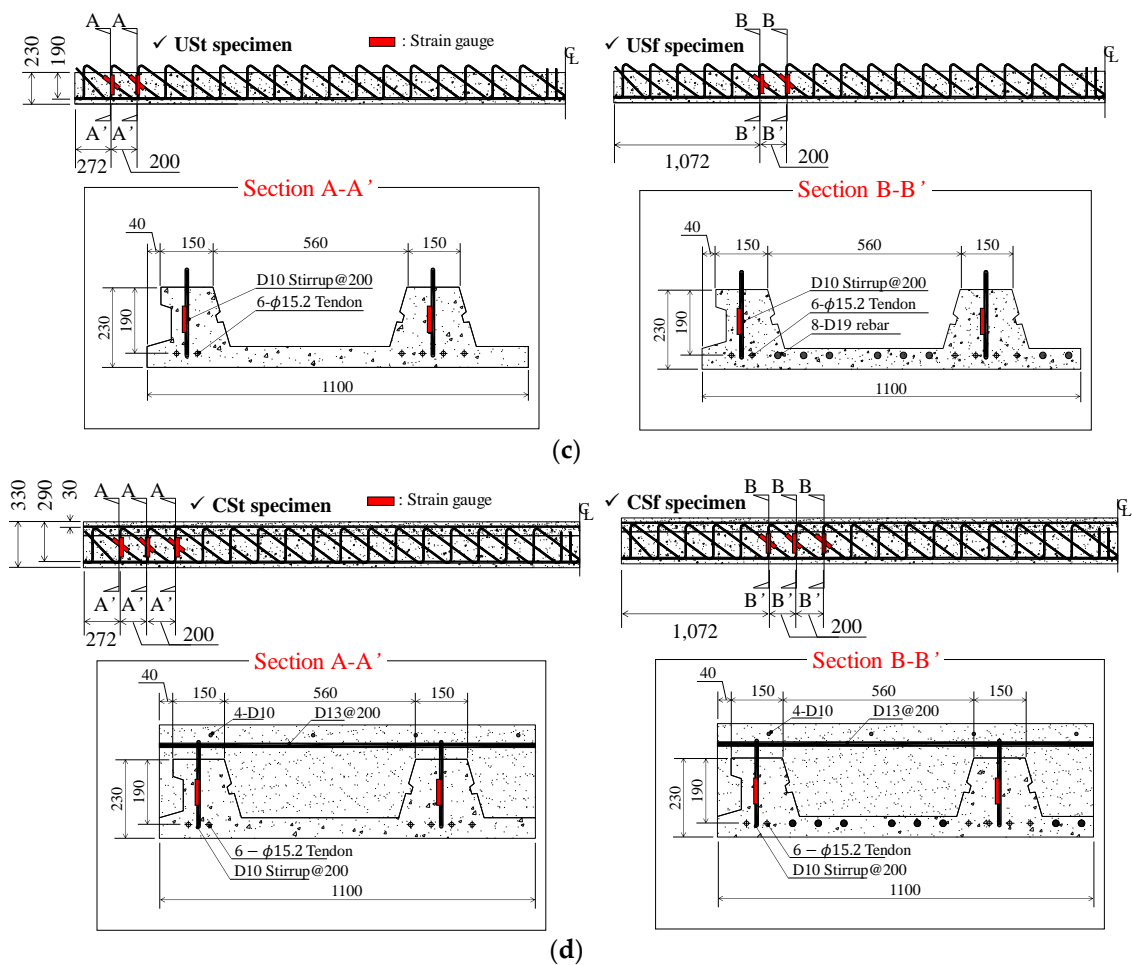


Figure 2. Details of test specimens (unit: mm); (a) UF specimen; (b) CF specimen; (c) USt and USf specimens; (d) CSf and CSs specimens.

As shown in Figure 2, in the UF specimen, strain gauges were attached to the strands on the tension side and concrete at the extreme compression fiber, whereas they were attached to the strands on the tension side and compression reinforcement in the CF specimen. Strain distributions in cross-sections according to loads were then measured in detail. For shear specimens, the shear contributions of the stirrups were measured by attaching gauges to the lattice bars placed in the test region.

2.2. Test Set-Up

Figure 3 shows the loading details of the test specimens. Two-point loading was applied to the simply supported UF and CF specimens, and one-point loading was applied to the US and CS specimens with a shear span to depth ratio (a/d_s) of 2.5. For the shear specimens, the left and right span lengths were set differently to induce shear failure in the target region. The deflections of the specimens were measured using linear variable differential transformers (LVDTs) installed at the center of the span of the flexural specimens, and the bottom of the cross-section located at the loading point of the shear specimens.

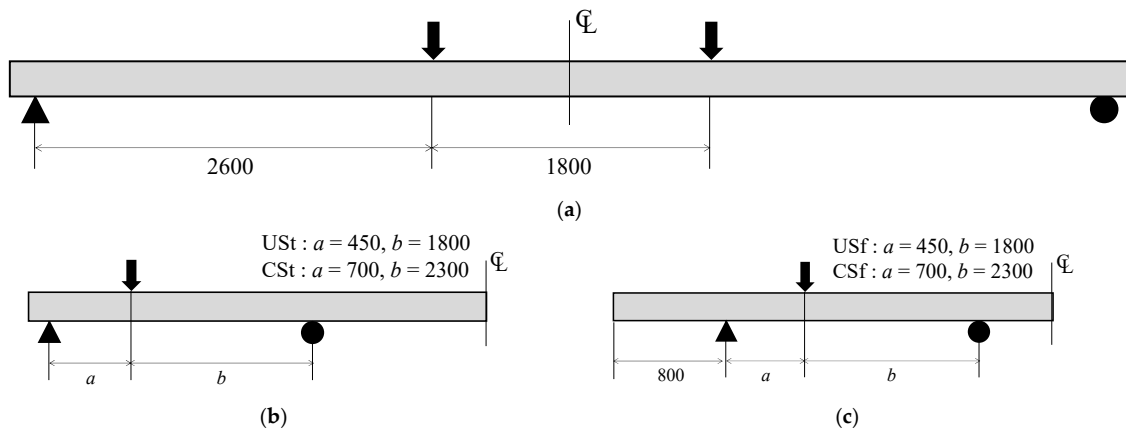


Figure 3. Test set-up (unit: mm); (a) UF and CF specimens; (b) USt and CSt specimens; (c) USf and CSf specimens.

3. Experimental Results

3.1. Failure Modes of the Test Specimens

Figure 4 shows the crack patterns of specimens at failure. The UF specimen, which is a PC unit slab without cast-in-place concrete, failed because of the sudden crushing of a rib on the compression side after flexural cracks had formed around the loading point. On the other hand, the CF specimen exhibited a typical flexural failure mode because of the crushing of concrete on the compression side after several flexural cracks propagated in the region of the maximum flexural moment. Meanwhile, both the USt and USf specimens underwent shear failure as web-shear cracks propagated at the ribs. However, as shown in Figure 4c,d, the shear crack angle generated in the USt specimen was steeper than that observed in the USf specimen, because the effective prestress (f_{se}) of the USt specimen is smaller than that of the USf specimen as the shear span of the USt specimen is located within the transfer length zone. The CSt and CSf specimens with case-in-place concrete showed a crack behavior different from that of the PC unit specimens. That is, inclined cracks occurred near the loading section with a relatively large flexural moment, and horizontal cracks towards the support were observed along with the interface between the PC unit slab and the cast-in-place concrete. In addition, the angle of the shear crack was about 60° , which was steeper than the shear crack angle ranging from 35° to 40° [16] that is generally observed in prestressed concrete (PSC) members. This is because the sectional area of cast-in-place concrete is considerably larger than that of the PC unit, and no prestressing is introduced to the cast-in-place concrete. Consequently, it is estimated that the effect resulting from the introduction of prestressing is lower than in the PC unit specimens.

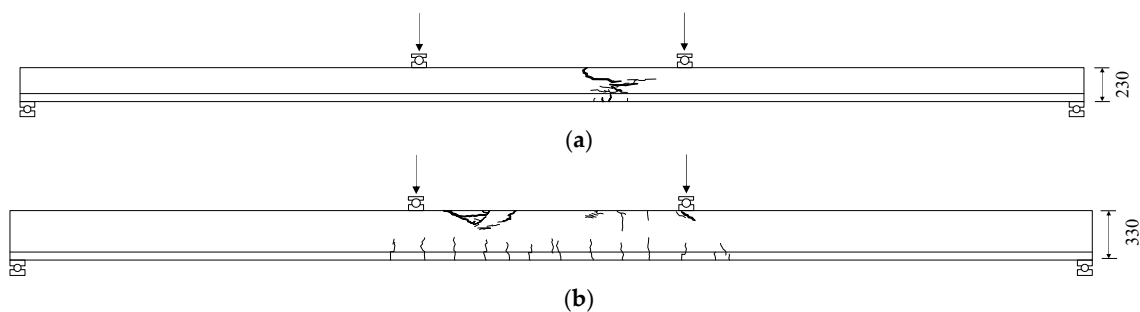


Figure 4. Cont.

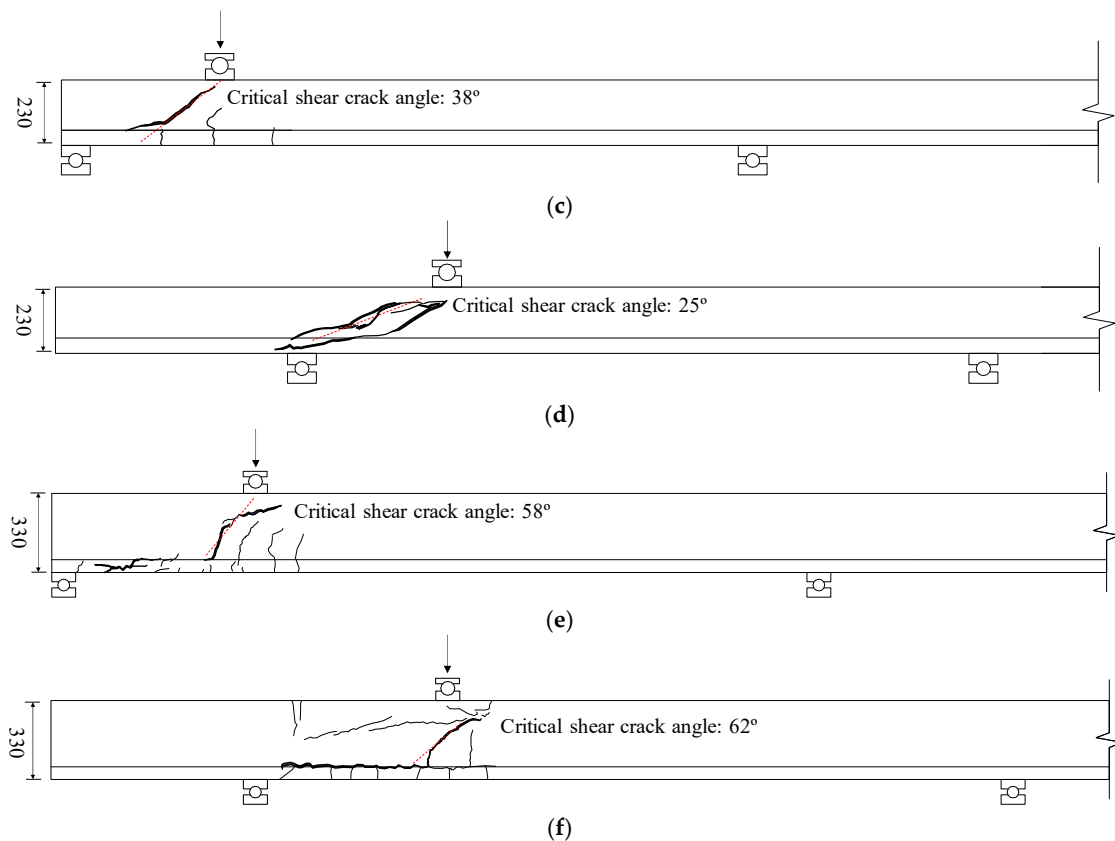


Figure 4. Crack patterns of test specimens at failure; (a) UF specimen; (b) CF specimen; (c) USt specimen; (d) USf specimen; (e) CSt specimen; (f) CSf specimen.

3.2. Load-Deflection Responses

Figure 5 shows the load-deflection curves of UF and CF specimens, and Table 2 summarizes the test results. In the UF specimen, which is a PC unit slab, the initial flexural crack was observed at a load of about 70 kN ($M_{cr} = 100.0$ kN·m). Later, flexural failure occurred as the concrete on the compression side in the upper part of the rib was crushed at a load of 96.2 kN ($M_u = 125.1$ kN·m). In the CF specimen, which is a composite member, flexural cracks were observed at a load of 147 kN ($M_{cr} = 191.5$ kN·m). Then, the stiffness of the specimens continued to be reduced, and flexural failure occurred at a load of 267.1 kN ($M_u = 347.2$ kN·m). The UF specimen showed slightly less ductility than the CF specimen; although the compressive force generated by the flexural moment should be resisted by the ribs in a UF specimen, the rib is very small narrow to the overall width of the member, as shown in Figure 2a, so that the position of the neutral axis is relatively low.

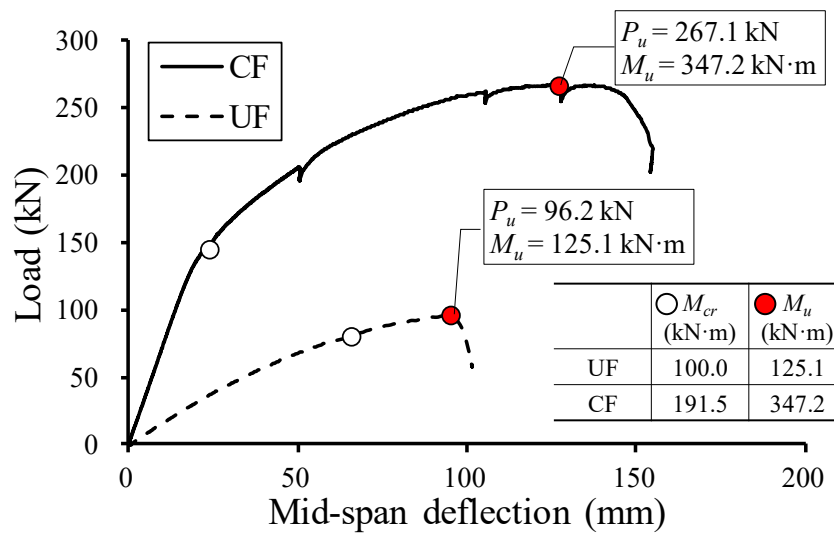


Figure 5. Load-deflection responses of flexural test specimens.

Table 2. Summary of test results.

Specimen	Failure Mode	Failure Loads (P_u , kN)	Flexural Strength (M_u , kN·m)	Shear Strength (V_u , kN)
UF	Flexure	96.2	125.1	-
CF	Flexure	267.1	347.2	-
USt	Shear	291.0	-	232.8
USf	Shear	325.6	-	260.5
CSt	Shear	548.0	-	420.1
CSf	Shear	848.8	-	650.7

Figure 6 shows the load-deflection curves of the USt, USf, CSt, and CSf specimens. In the USt specimen tested in the transfer length zone of the PC unit slab, shear cracks were observed at a load of about 151 kN ($V_{cr} = 121$ kN), and shear failure occurred at a load of 291 kN ($V_u = 233$ kN). In the USf specimen tested in the strain plateau zone of the PC unit slab, the initial shear crack occurred at a load of about 170 kN ($V_{cr} = 136$ kN). Even after that, new shear cracks were formed, as shown in Figure 4d, and shear failure occurred at a load of 326 kN ($V_u = 261$ kN). However, unlike the USt specimen, there was no decrease in the stiffness of the member, even after shear cracking, in the USf specimen. On the CSt specimen, which is a composite member, flexural cracks around the loading point developed into inclined shear cracks at a load of about 370 kN ($V_{cr} = 284$ kN), and shear failure took place as the horizontal crack towards the support along the interface between the PC unit slab and cast-in-place concrete occurred at a load of 548 kN ($V_u = 420$ kN). In the CSf specimen, the initial inclined crack was observed at a load of 420 kN ($V_{cr} = 322$ kN), and shear failure took place as the horizontal crack towards the support occurred at a load of 849 kN ($V_u = 651$ kN) similarly to that in the CSt specimen. As can be seen from the test results, the shear cracking strength (V_{cr}) and ultimate shear strength (V_u) of the USf and CSf specimens tested in the strain plateau zone, where the effective prestress (f_{se}) is fully developed, were found to be greater than those of the USt and CSt specimens, respectively.

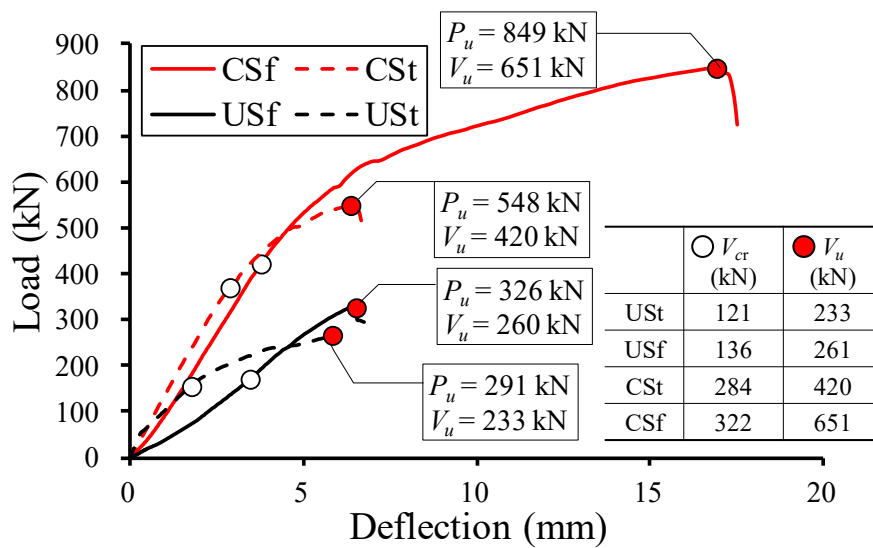


Figure 6. Load-deflection responses of shear test specimens.

3.3. Measured Strains

Figure 7a,b shows the strain distributions of the sections measured at the regions of the UF and CF specimens with maximum moment. In the UF specimen, the position of the neutral axis was raised with increasing loads, and the strain in concrete at the compression edge was close to the ultimate strain ($\epsilon_{cu} = 0.003$) at a load ($0.95P_u$), where P_u is the failure load. However, the strain in strands did not increase as much as did the strain in concrete at the compression edge, because the ribs are very narrow in the PC unit slab, and thus the neutral axis position is low. Accordingly, the member was found to be not very ductile. On the other hand, the CF specimen, which has a sufficient compressive resistance area because of the presence of cast-in-place concrete, exhibited a large tensile strain of the strand at flexural failure and demonstrated highly ductile behavior.

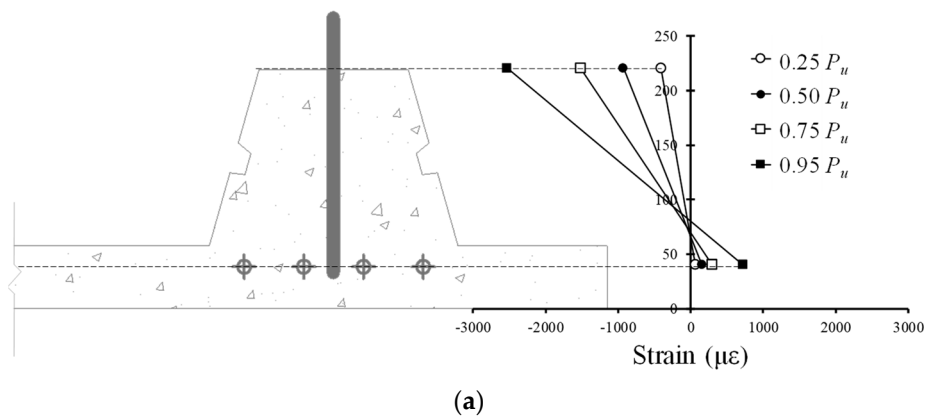


Figure 7. Cont.

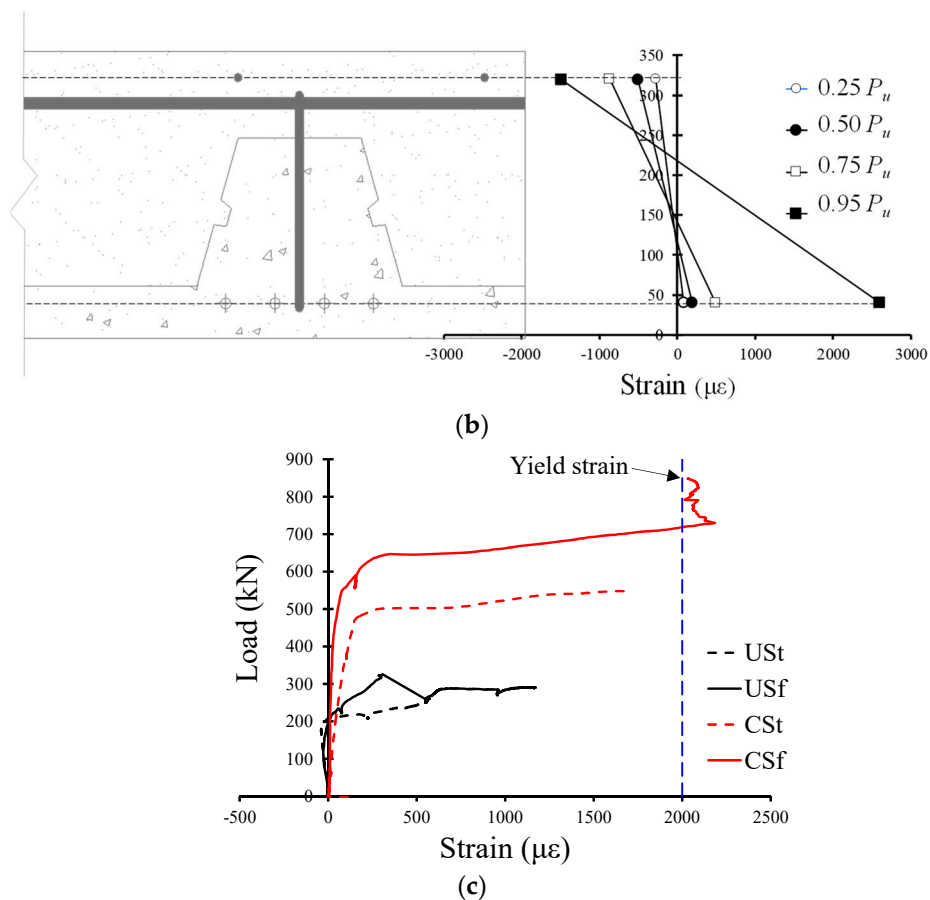


Figure 7. Measured strains from test specimens; (a) Strain distribution in the section located at maximum moment region (UF specimen); (b) Strain distribution in the section located at the maximum moment region (CF specimen); and (c) Stirrup strains measured from the shear test specimens.

Figure 7c shows the strains measured from stirrups placed in the shear specimens. In the PC unit specimens (USf and USf), the stirrup made a partial contribution to the shear resistance of the member but did not yield even at the maximum load. This is because the embedment length of the stirrup is short in the PC unit slab, and the hook at the top protrudes before the placement of cast-in-situ concrete. It should be noted that the shear reinforcement in the JAS member is designed not to secure the shear performance of the PC unit slab but to ensure the shear performance of composite members. On the other hand, composite specimens (CSf and CSf) with cast-in-place concrete, in which shear reinforcement is properly anchored in the cross-section, exhibited a strain close to the yield strain after shear cracking and effectively contributed to the shear resistance of the member.

4. Analysis of Flexural Behavior and Shear Strength

4.1. Non-Linear Flexural Analysis

In this study, a layered analysis [17,18] shown in Figure 8a was performed to evaluate the flexural behavior of the JAS. Since no damage at the interface between the PC unit slab and cast-in-place concrete was observed in the CF specimen, the PC and the cast-in-place concrete were considered to be fully composite in the flexural analysis. On the assumption of strain in concrete at the compression edge (ϵ_t) and neutral axis depth (c), the strain of compression reinforcement (ϵ'_s), the strain of strands (ϵ_{ps}), and the concrete strain ($\epsilon_{c,i}$) in each layer can be calculated through the compatibility conditions. Then the stresses corresponding to each strain can be obtained from the constitutive laws for steel and concrete materials shown in Figure 8b. In this study, the Collins model [19], the elasto-perfectly

plastic model [20,21], and Ramberg–Osgood model [22,23] were adopted as the constitutive equations of the concrete, reinforcing bars, and strands, respectively. The compression force of the PC (C_{PC}), of the cast-in-place concrete (C_{RC}), and of the reinforcement (C_s), and tension force of strands (T_{ps}) can be calculated by multiplying the stress and areas of each element, and the moment-curvature response can be obtained from iterative calculations performed until the conditions for equilibrium of forces (i.e., $C_{PC} + C_{RC} + C_s + T_{ps} \approx 0$) are satisfied. In addition, the load-deflection response can be derived from the numerical integration of the curvature (ϕ_i) for each section, as shown in Figure 8c. A numerical calculation example can be found in Appendix A.

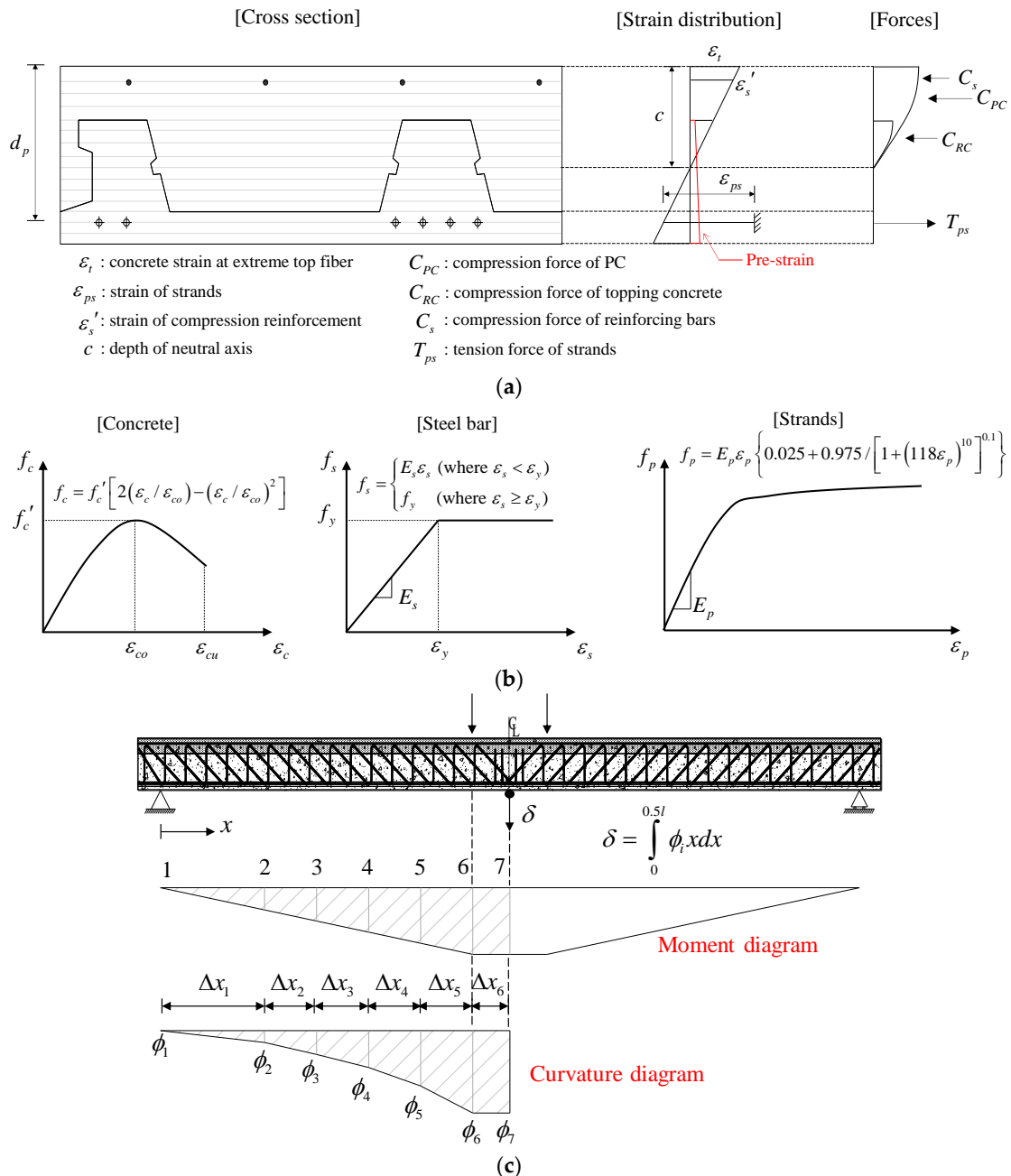


Figure 8. Non-linear flexural analysis; (a) Layered analysis model; (b) Constitutive laws of materials; (c) Numerical integration for estimating mid-span deflection.

4.2. Estimation of Shear Strength

Table 3 shows code equations for estimating the shear strength presented in ACI 318-14 [11], which were applied to evaluate the shear performance of the JAS. As mentioned earlier, shear reinforcement placed in the US series specimens without cast-in-place concrete did not contribute effectively to the shear resistance of the member. Therefore, only the contribution of the concrete (V_{cw}) was taken into account in estimating the shear strength of the PC unit members, without regard for the contribution of the shear reinforcement (V_s). Meanwhile, the compressive strengths of the PC unit and cast-in-place concrete are different in composite members, and ACI 318-14 [11] specifies that it is allowable to use the material properties of the elements that result in the most critical value of shear strength (V_n). However, in this case, it tends to be very conservative in evaluating the shear strength of the member. In addition, if the web shear strength equation for prestressed concrete members (V_{cw}) is applied to get the web shear strength of JAS members, it causes the fallacy that prestress is effective in all cross-sections including the cast-in-place concrete, while prestress force is introduced only to the PC unit in the JAS. Consequently, this approach provides an unsafe estimation on the shear strength of JAS members. For this reason, a way to estimate the shear strength by considering the entire composite PC slab to be reinforced concrete (RC) in order to achieve the safe side design has often been applied in practice [12].

Table 3. Code equations for estimating shear strength [11].

Term	Equations
Shear strength of reinforced concrete (V_c)	$V_c = 0.17 \sqrt{f'_c} b_w d_s$
Web shear strength of prestressed concrete (V_{cw})	$V_{cw} = (0.29 \sqrt{f'_c} + 0.3 f_{pc}) b_w d_p$, where $f_{pc} = \frac{f_{se} A_{ps}}{A_{pc}}$
Shear contribution of stirrups (V_s)	$V_s = \frac{A_v f_{vy} d_s}{s_v} (\sin \alpha \cot \beta + \cos \alpha)$

* Notations: b_w : web width, d_s : effective depth of tension reinforcement, d_p : effective depth of prestressing strands, f'_c : compressive strength of concrete, f_{se} : effective prestress, A_{pc} : sectional area of prestressed member, A_{ps} : sectional area of prestressing strands, A_v : sectional area of the stirrup, f_{vy} : yield strength of the stirrup, s_v : spacing of stirrups, α : inclined angle of the stirrup, β : angle of critical shear crack.

In this study, the shear strength (V_n) of the composite member was estimated by three methods (labeled Methods 1, 2, 3), as shown in Figure 9. Note that the area indicated in red is where the shear strength is estimated by regarding the composite member to be PSC, whereas the area indicated in blue is where the shear strength is estimated by regarding it as being RC. Method 1 is a method for calculating the shear contribution (V_{cw}) by defining the distance from the compression edge of the composite member to the center of the strands layer as d_p , and estimating the shear strength by considering the remaining part as RC. On the other hand, Method 2 estimates V_{cw} by considering the distance from the top of the PC unit rib to the center of the strands layer as d_p . Method 3 estimates the shear strength by regarding the cross-section as being RC. According to the test results, the stirrup effectively contributed to the shear resistance mechanism in the composite member. Therefore, the contribution of the shear reinforcement (V_s) was taken into consideration in the estimation of the shear strength. However, since the critical shear crack angle (β) observed in the test specimens was distributed in the range from 58° to 62°, β was applied at 60° in the estimation of V_s .

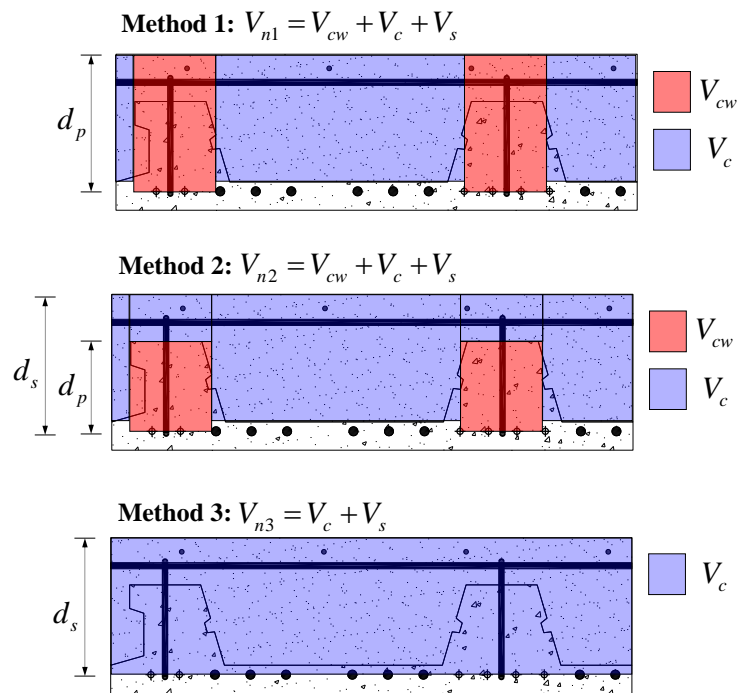


Figure 9. Shear strength estimation methods for composite member.

4.3. Comparison of Test and Analysis Results

Figure 10 compares the test and non-linear flexural analysis results of the UF and CF specimens. It was found that the analysis model provides very approximate predictions of the flexural strength and behavior of the specimens, and thus, can be applied to the flexural design of the JAS.

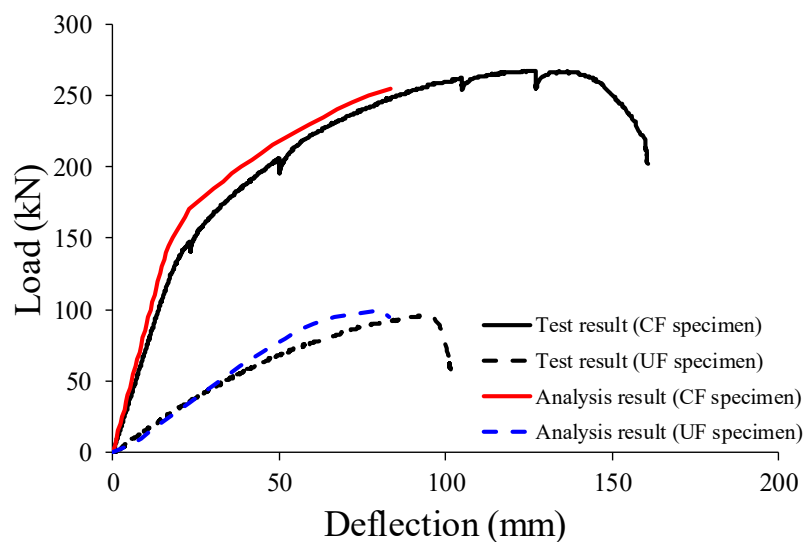


Figure 10. Comparison of the test and analysis results on the flexural specimens.

Figure 11 and Table 4 compare the test and analysis results of the shear specimens (US and CS series). As shown in Figure 11a, for the PC unit specimens, the shear strength estimation method, considering only the contribution of concrete (V_{cw}) without regard for the contribution of the shear reinforcement (V_s), provided the conservative calculation results. For the composite specimens, Method 1 (V_{n1}), which applies the effective depth (d_p) of the composite member, including the thickness of the topping slab in the upper part of the rib, provided the analysis results of the unsafe side, whereas Method 3 (V_{n3}), which estimates the shear strength by considering the gross-section to be RC, evaluated

the shear strength of the composite specimens to be on the excessively safe side. Meanwhile, Method 2 (V_{n2}), which calculates V_{cw} by regarding the distance from the top of the PC unit rib to the center of the strands layer as d_p , slightly overestimated the shear strength of the CSt specimen, but provided a much more reasonable evaluation of the shear strength of composite members when compared to Methods 1 or 2. Considering that the safety factor and strength reduction factor are applied in the practical design, the most economical and reasonable design can be derived by using Method 2 when estimating the shear strength of the composite JAS. In this case, it is appropriate to apply 60° as the angle of the shear crack for estimating the contribution of the shear reinforcement (V_s).

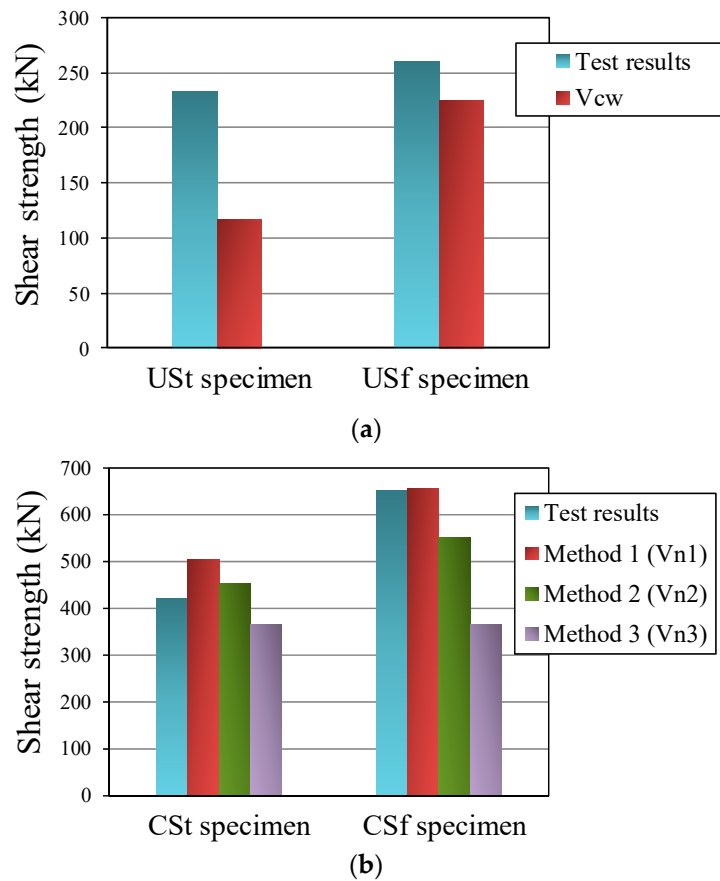


Figure 11. Comparison of the test and analysis results on the shear specimens; (a) Non-composite members; (b) Composite members.

Table 4. Comparison of shear strengths.

Specimen	Test Results (V_u , kN)	Calculation Results (V_n , kN)		
		V_{n1} (Ratio, V_u/V_{n1})	V_{n2} (Ratio, V_u/V_{n2})	V_{n3} (Ratio, V_u/V_{n3})
USt	232.8		115.9 (2.01)	
USf	260.4		223.9 (1.16)	
CSt	420.3	504.8 (0.83)	452.7 (0.93)	364.7 (1.15)
CSf	651.2	655.9 (0.99)	551.7 (1.18)	364.7 (1.78)

5. Conclusions

In this study, experimental and analytical research has been performed to evaluate the flexural and shear performance of the half-precast concrete slab with inverted multi-ribs (Joint Advanced Slab, JAS). The crack patterns, load-deflection responses, and strain behavior of the longitudinal and shear

reinforcement of the specimens were measured and analyzed in detail, and the flexural and shear performance of the JAS was quantitatively evaluated using a non-linear flexural analysis method and ACI 318-14 code. In addition, a design method that can most reasonably estimate the shear strength of the JAS was proposed based on the test results. On this basis, the following conclusions can be drawn:

1. The UF specimen, a PC unit slab, exhibited a ductility slightly lower than that of the CF specimen with cast-in-place concrete; although the compressive force generated by the flexural moment should be resisted by the ribs, the rib is much narrower than the overall width of the member, and thus the position of the neutral axis is relatively low.
2. The non-linear flexural analysis provided very approximate evaluations of the flexural behavior and strength of the JAS, regardless of the presence of cast-in-place concrete, and thus can be applied to the flexural design of the JAS.
3. The shear test results showed that the lattice reinforcement placed in composite specimens exhibited effective shear resistance performance, whereas the lattice reinforcement placed in PC unit specimens did not make a significant contribution to the shear resistance of the member. Therefore, the shear design results of the safe side can be obtained without considering the contribution of shear reinforcement (V_s) in the design of the PC unit slab.
4. The shear crack angle observed in composite specimens was about 60° , which was steeper than that observed in the general PSC member. In addition, various methods for estimating the shear contributions of the PC unit and cast-in-place concrete were examined based on the ACI 318-14 code. The results confirmed that a method of calculating the contribution of shear reinforcement (V_s) by applying the crack angle (β) of 60° , and estimating the PC unit shear contribution (V_{cw}) by regarding the distance from the top of the PC unit rib to the center of the strands layer as the effective depth (d_p) of the composite member, while estimating the shear strength by considering the remaining part as RC, provides the most reasonable analysis results.

Author Contributions: Original draft manuscript—S.-J.H.; Validation—J.-H.J. and H.-E.J.; Investigation—S.-H.C. and S.C.; Supervision and Review Writing—K.S.K.

Funding: This research received no external funding.

Acknowledgments: This work was supported by the National Research Foundation of Korea (NRF) grant funded by the Korea government (MSIT) (No. 2019R1A2C2086388).

Conflicts of Interest: The authors declare no conflict of interest.

Appendix A

In this section, an example of numerical calculations on the flexural behavior of composite JAS is presented. The sectional details and material properties of JAS are shown in Figure 2b and Table 1, respectively.

- **Input parameters** (Figure A1):

$$h_{pc} = 230 \text{ mm}, h_{top} = 100 \text{ mm}, d_p = 290 \text{ mm}, d'_s = 40 \text{ mm}, b = 1100 \text{ mm}, b_w = 150 \text{ mm}$$

$$f'_{c,pc} = 36.0 \text{ MPa}, f'_{c,rc} = 21.3 \text{ MPa}, f_y = 503 \text{ MPa}, f_{pu} = 1936 \text{ MPa}, f_{se} = 0.61 f_{pu}$$

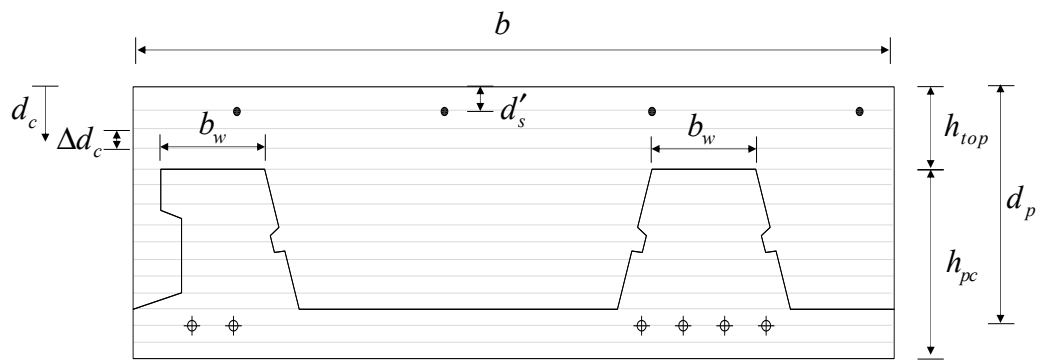


Figure A1. Section details of JAS.

-Moment-curvature response

Step 1: Select $\epsilon_t = -0.001$

Step 2: Assume $c = 100$ mm

Step 3: Obtain the distribution of strains, as shown in Figure A2.

$$\epsilon_b = \frac{c - (h_{pc} + h_{top})}{c} \times \epsilon_t = 0.0026,$$

$$\epsilon'_s = \frac{c - d'_s}{c} \times \epsilon_t = -0.00099, \text{ and } \epsilon_{ps} = \frac{f_{se}}{E_s} + \frac{c - d_p}{c} \times \epsilon_t = 0.0076$$

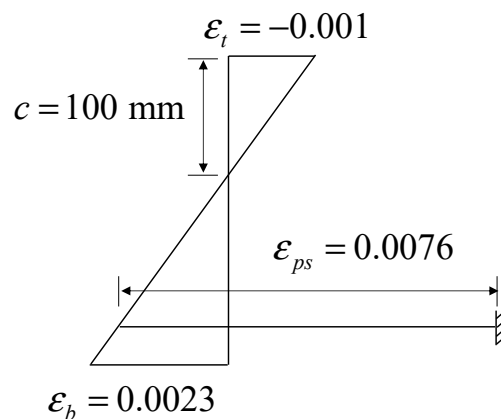


Figure A2. Strain distribution

Step 4: Calculate stresses of concrete layers, strands, and compressive reinforcement from constitutive laws of materials shown in Figure 8b.

Step 5: Calculate forces of concrete, strands, and compressive reinforcement.

$$C_{pc} = \sum f_{c,pc} \cdot b_i \cdot \Delta d_c = 15.1 \text{ kN}$$

$$C_{RC} = \sum f_{c,rc} \cdot b_i \cdot \Delta d_c = -732.4 \text{ kN}$$

$$C_s = f'_s A'_s = -56.5 \text{ kN}$$

$$T_{ps} = f_{ps} A_{ps} = 1258.8 \text{ kN}$$

Step 6: Check force equilibrium.

$$C_{pc} + C_{RC} + C_s + T_{ps} \neq 0 \text{ (Not satisfied)}$$

Step 7: Go back to the step 2, and update c until the force equilibrium is satisfied.

If the neutral axis depth (c) is assumed to be 135 mm, the forces of concrete, strands and compressive reinforcement are calculated, as follows:

$$C_{pc} = -119.4 \text{ kN}, C_{RC} = -953.1 \text{ kN}, C_s = -56.6 \text{ kN}, T_{ps} = 1136.0 \text{ kN}$$

The equilibrium condition is also satisfied, $C_{pc} + C_{RC} + C_s + T_{ps} = 6.9 \text{ kN} \approx 0$.

Step 8: Calculate curvature (ϕ) and moment (M).

$$\phi = \frac{\epsilon_t}{c} = 7.4 \times 10^{-6}$$

$$M = \sum f_{c,pc} \cdot b_i \cdot d_c \cdot \Delta d_c + \sum f_{c,rc} \cdot b_i \cdot d_c \cdot \Delta d_c + f'_s A'_s d'_s + f_{ps} A_{ps} d_p = 276.3 \text{ kN}\cdot\text{m}$$

Step 9: Repeat step 1 to 8 with an updated ϵ_t until ϵ_t reaches the crushing strain of concrete (-0.003). The moment-curvature response of composite JAS is presented in Figure A3:

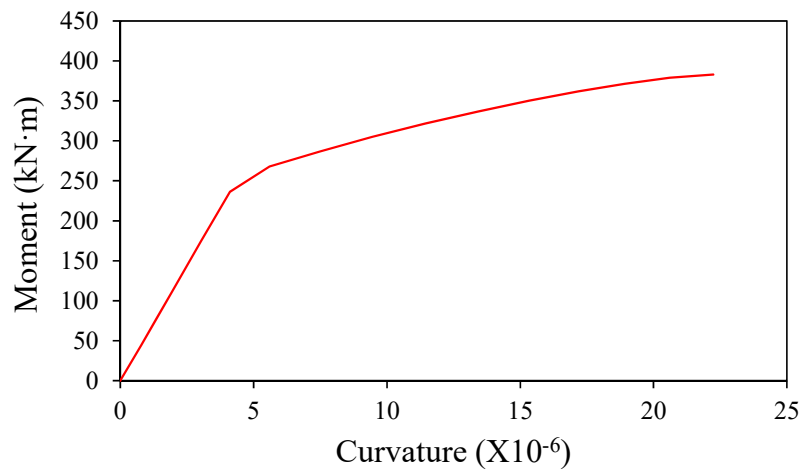


Figure A3. Moment-curvature response.

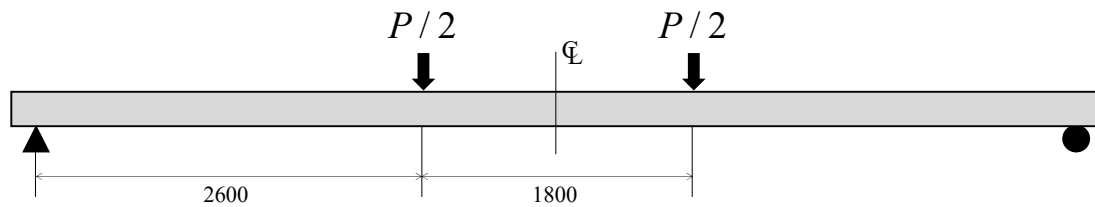


Figure A4. Loading details.

-Load-deflection response.

The loading details of JAS is shown in Figure A4.

Step 1: Select $P = 50 \text{ kN}$.

Step 2: Obtain moment and curvature distributions from Figure A3.

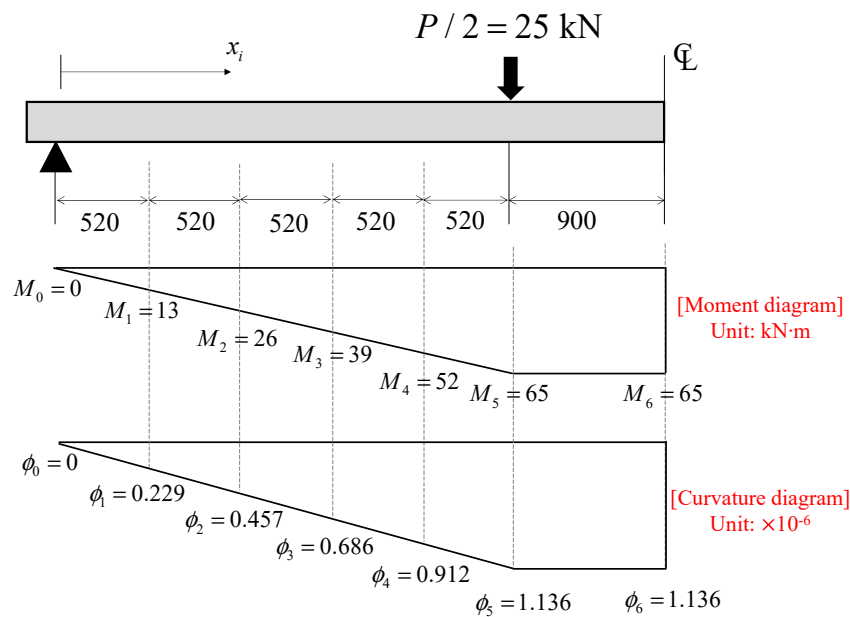


Figure A5. Moment and curvature distributions.

Step 3: Calculate mid-span deflection by numerically integrating curvatures shown in Figure A5, as follows:

$$\delta = \int_0^{0.5l} \phi_i x dx = \left(\frac{\phi_0 x_0 + \phi_1 x_1}{2} \right) \Delta x_0 + \left(\frac{\phi_1 x_1 + \phi_2 x_2}{2} \right) \Delta x_1 + \dots + \left(\frac{\phi_5 x_5 + \phi_6 x_6}{2} \right) \Delta x_5 = 5.73 \text{ mm}$$

Step 4: Repeat step 1 to 3 with updating P , then the load-deflection response can be obtained, as shown in Figure 10.

References

- Ju, H.; Han, S.J.; Choi, I.S.; Choi, S.; Park, M.K.; Kim, K.S. Experimental study on an optimized-section precast slab with structural aesthetics. *Appl. Sci.* **2018**, *8*, 1234. [CrossRef]
- Kim, S.E.; Colin, J. *Multi-Story Precast Concrete Framed Structures*, 2nd ed.; Wiley-Blackwell: Hoboken, NJ, USA, 2014; Available online: <https://www.wiley.com/en-us/Multi+Storey+Precast+Concrete+Framed+Structures%2C+2nd+Edition-p-9781405106146> (accessed on 8 March 2019).
- Lee, D.H.; Park, M.K.; Oh, J.Y.; Kim, K.S.; Im, J.H.; Seo, S.Y. Web-shear capacity of prestressed hollow-core slab unit with consideration on the minimum shear reinforcement requirement. *Comput. Concr.* **2014**, *14*, 211–231. [CrossRef]
- Newell, S.; Goggins, J.; Hajdukiewicz, M.; Holleran, D. Behaviour of hybrid concrete lattice girder flat slab system using insitu structural health monitoring. In Proceedings of the Civil Engineering Research in Ireland Conference (CERI 2016), Galway, Ireland, 29–30 August 2016.
- Hou, H.; Liu, X.; Qu, B.; Ma, T.; Liu, H.; Feng, M.; Zhang, B. Experimental evaluation of flexural behavior of composite beams with cast-in-place concrete slabs on precast prestressed concrete decks. *Eng. Struct.* **2015**, *126*, 405–416. [CrossRef]
- Yang, L. Design of prestressed hollow core slabs with reference to web shear failure. *J. Struct. Eng.* **1994**, *120*, 2675–2696. [CrossRef]
- Palmer, K.D.; Schultz, A.E. Factors affecting web-shear capacity of deep hollow-core units. *PCI J.* **2010**, *55*, 123–146. [CrossRef]
- Palmer, K.D.; Schultz, A.E. Experimental investigation of the web-shear strength of deep hollow-core units. *PCI J.* **2011**, *56*, 83–104. [CrossRef]
- Pisanty, A. The shear strength of extruded hollow-core slabs. *Mater. Struct.* **1992**, *25*, 224–230. [CrossRef]

10. Im, J.H.; Park, M.K.; Lee, D.H.; Kim, K.S.; Seo, S.Y. *Evaluation of Web-Shear Capacity of Thick Hollow-Core Slabs*; The Regional Association of Architectural Institute of Korea: Daegu, Korea, 2014; Volume 16, pp. 139–145. Available online: https://aikra.jams.or.kr/co/com/EgovMenu.kci?s_url=/sj/search/sjSereClasList.kci&s_MenuId=MENU-00000000053000 (accessed on 21 March 2019). (In Korean)
11. ACI Committee 318. *Building Code Requirements for Reinforced Concrete and Commentary*; ACI 318-14; American Concrete Institute: Farmington Hills, MI, USA, 2014.
12. Ju, H.; Han, S.J.; Joo, H.E.; Cho, H.C.; Kim, K.S.; Oh, Y.H. Shear performance of optimized-section precast slab with tapered cross section. *Sustainability* **2019**, *11*, 163. [[CrossRef](#)]
13. Naito, C.; Cao, L.; Peter, W. Precast concrete double-tee connections, part 1: Tension behavior. *PCI J.* **2009**, *54*, 49–66. [[CrossRef](#)]
14. Cao, L.; Naito, C. Precast concrete double-tee connectors, part 2: Shear behavior. *PCI J.* **2009**, *54*, 97–115. [[CrossRef](#)]
15. Rubene, S.; Vilnitis, M. Impact of low temperatures on compressive strength of concrete. *Int. J. Theor. Appl. Mech.* **2017**, *2*, 97–101.
16. Collins, M.P.; Mitchell, D. *Prestressed Concrete Structures*; Prentice-Hall: Upper Saddle River, NJ, USA, 1991.
17. Lee, D.H.; Han, S.J.; Joo, H.E.; Kim, K.S. Control of tensile stress in prestressed concrete members under service loads. *Int. J. Concr. Struct. Mater.* **2018**, *12*, 38. [[CrossRef](#)]
18. Han, S.J.; Lee, D.H.; Oh, J.Y.; Choi, S.H.; Kim, K.S. Flexural responses of prestressed hybrid wide flange composite girders. *Int. J. Concr. Struct. Mater.* **2018**, *12*, 53. [[CrossRef](#)]
19. Vecchio, F.J.; Collins, M.P. The modified compression-field theory for reinforced concrete elements subjected to shear. *ACI J. Proc.* **1986**, *83*, 219–231. [[CrossRef](#)]
20. Scholz, H. Ductility, redistribution, and hyperstatic moments in partially prestressed members. *ACI Struct. J.* **1990**, *87*, 341–349. [[CrossRef](#)]
21. Rodriguez-Gutierrez, J.A.; Aristizabal-Ochoa, J.D. Partially and fully prestressed concrete sections under biaxial bending and axial load. *ACI Struct. J.* **2000**, *97*, 553–563. [[CrossRef](#)]
22. Mattock, A.H. Flexural strength of prestressed concrete sections by programmable calculator. *PCI J.* **1979**, *24*, 32–54. [[CrossRef](#)]
23. Park, H.; Cho, J.Y. Ductility analysis of prestressed concrete members with high-strength strands and code. *ACI Struct. J.* **2017**, *114*, 407–416. [[CrossRef](#)]



© 2019 by the authors. Licensee MDPI, Basel, Switzerland. This article is an open access article distributed under the terms and conditions of the Creative Commons Attribution (CC BY) license (<http://creativecommons.org/licenses/by/4.0/>).